PACKAGING TECHNOLOGY AND SCIENCE
Packag. Technol. Sci. **12**, 161–171 (1999)

Evaluation of Defects in the Seal Region of Food Packages Using the Ultrasonic Contrast Descriptor, ΔBAI

By Ayhan Ozguler, Scott A. Morris and William D. O'Brien, Jr.*

A rapid, dependable method of on-line package inspection will allow wider implementation of energy- and material-efficient retortable pouches and trays, by reducing inspection costs. To evaluate high-frequency ultrasonic imaging as a sensing method, the 17·3 MHz ultrasonic pulse-echo Backscattered Amplitude Integral (BAI) method was used to visualize and evaluate major defects (channels and product inclusions, which compromise the seal integrity and must be reliably inspected) in the seal area of flexible food packages. The focus of this study was to evaluate the image contrast, denoted ΔBAI, for various packaging materials, defect types and sizes. Channel (6–100 μm in diameter) and inclusion defects (strands of mouse tail tendons, 20–150 μm) were created in the seal area of all-plastic and foil-containing packaging films. It has been shown that there is a direct relationship between the defect size and ΔBAI value, and that different defect types and packaging materials have a significant impact on the ΔBAI value. The utility of ΔBAI for detecting defects makes it a useful and reliable sensing method for package inspection. Copyright © 1999 John Wiley & Sons, Ltd.

Received 14 February 1999; Accepted 7 April 1999

KEY WORDS: seals; channel defects; ultrasound; pulse-echo; BAI-mode imaging

INTRODUCTION

Retortable pouches use thermal-resistant films made of layers of plastic and foil in which the food is retorted, just as with canned products, to extend shelf life. After the package is filled, it is sealed by means of a fusion weld of two compatible polymeric film surfaces and then commercially sterilized in a pressurized steam retort. A good fusion seal prevents the post-process contamination of the food product.[1–3] Any compromise of the seal fusion area may cause recontamination or leakage.

There are two critical defects found in the seal regions of such packages: channel leaks and weak seals.[4] Channel leaks cause pathways for microbial penetration that eventually result in spoilage of the product. The weak seal that is generally caused by wrinkles, surface irregularities, delamination and product involvement in the seal area causes the seal strength to decrease, and that gives rise to product deterioration during storage.[1] Because both types of defect may bring about health hazards and product loss, it is imperative that packaging be checked for the presence of such defects

Package integrity testing is divided into two main categories: destructive and non-destructive tests. Destructive tests used in the food industry include electrolytic, dye penetration, seal strength,

* Correspondence to: S. A. Morris, Department of Food Science and Human Nutrition, University of Illinois, 1304 W. Pennsylvania Avenue, Urbana, IL 61801, U.S.A.
Email: smorris@uiuc.edu
Contract/Grant Sponsor: Value-Added Research Opportunities Program, Agricultural Experiment Station, University of Illinois.

 CCC 0894–3214/99/040161–11 $17.50

burst and biological tests. Because these tests are slow, expensive and give only a statistical level of certainty,[3] they are unsatisfactory. On the other hand, non-destructive inspection can also ensure product safety and enable rapid detection of defects. Some of the non-destructive techniques that have been evaluated for seal integrity testing[5] are machine vision imaging, X-ray, eddy current probes, magnetic resonance imaging (MRI) and ultrasound. In this evaluation, it was indicated that none of these techniques was infeasible and that they had some application possibilities, but that ultrasound offers the best combination of accuracy, speed and safety.

A US patent[6] describes an *ultrasonic transmission technique* for testing the seal integrity of a package having a lid heat sealed to the container rim. The device detected large contaminating type defects such as silicon grease, teflon inclusions and meat in the seal region of the package. However, in this study no information was available about the detection of microscopic channel leaks which might permit microbial penetration.[3,4,7,8] Furthermore, the tests were run with approximately 1 mm^2 of meat fibre mix positioned in the seal region. Even though there is no official minimum size specification of any inclusion defect for package recontamination, the detected meat fibre in this study is much larger than that necessary to cause recontamination. In a recent study,[9] channel defects as small as 10 μm in diameter within the seal region of a polyethylene film and plastic microwaveable retort pouch have been reliably detected and imaged by using a Scanning Laser Acoustic Microscope (SLAM) at 100 MHz. SLAM also uses transmitting and receiving components like the device described in the US patent.

Unlike the transmission technique, the *ultrasonic pulse-echo technique* uses only one transducer for defect detection, which transmits the sound wave and receives the reflected wave produced by any discontinuities such as boundary layers between the material and coupling agent, inhomogeneities and flaws within the test material. A new technique called the Backscattered Amplitude Integral (BAI) method, which yields an image (the BAI-mode image) after the pulse-echo application has been introduced for detection of channel defects in the seal region of retort pouches.[10] In the US patent,[6] it was claimed that the pulse-echo technique would not adequately be sensitive to detect small defects ($\sim 1\ mm^2$) such as meat fibres and other food fibres within the seal region of the container. Contrary to this claim, the pulse-echo BAI-mode imaging technique at 17·3 MHz under oblique incidence conditions (7°) will reliably detect channel defects in the 10 μm range regardless of whether low impedance (air) or high impedance (water) material resides within the channel defect. Additionally, since the method is acoustic rather than optical, transparency, colour or printing of the material does not affect the results.

In a recent study,[11] the BAI-mode imaging technique at 17·3 MHz ultrasonic centre-frequency under normal incidence condition detected channel defects as small as 6 μm diameter in the seal region of both all-plastic and foil-containing pouch materials. In addition, strands of mouse tail tendon as small as 20 μm in diameter (used as a simulation of typical biomaterial such as meat or other food fibre which might be caught in the seal area) were successfully detected by the BAI-mode imaging technique.

Even though recent studies[7,8] showed that microbiological penetration occurred from 10 μm channel leaks in plastic pouches, it was argued that channel leaks smaller than 100 μm infrequently occur, and that subjecting food packages to extremely hostile environments such as biotesting is a huge exaggeration of actual hazardous situations. According to the several experts' opinion (discussed in Reference 4), detection of channel leaks as small as 50 μm in diameter by an in-line inspection system can provide an adequate safety assurance, in spite of penetration of 0·8 μm holes by organisms under pressure in the laboratory. The lack of a standard or official minimum size is a hindrance to the development of inspection methodologies. In addition, the inspection for such defects is mandated by the USDA (US Code of Federal Regulations (9CFR§381.301(d)[12]—the most stringent in this regard, and thus the limiting factor in production), and human ocular resolution is approximately 50 μm under the best of conditions.[13] Thus, the ultrasonic BAI-imaging technique already exceeds the resolution and accuracy of human inspectors who are satisfying the inspection requirement, although it does not yet do so at production speeds.

A contrast descriptor for the channel defect on a BAI-mode image was described in Reference 10,

Table 1. Physical properties of packaging materials used in the experiment

Packaging material	All-plastic trilaminate film			Foil-containing trilaminate film		
Layers	Inner	Middle	Outer	Inner	Middle	Outer
Layer material	PP*	PVDC*	ON*	PP*	AF*	PE*
Thickness (μm)	80	15 110	15	NA*	NA* 120	NA*
Density (kg/m^3)	900†	1 600–1 700†	1 140†	900†	2 700‡	1 400†
Sound speed (m/s)	2 660‡	2 380‡ 2 380§	2 600‡	2 660‡	6 420‡ 2 460§	2 340‡

* PP = polypropylene; PVDC = polyvinylidene chloride; ON = orientated nylon, 6/6; AF = aluminium foil; PE = polyester; NA = not available.
† Data obtained from Reference 15.
‡ Data obtained from Reference 16.
§ Measured in the laboratory.

and was named ΔBAI. It is calculated by subtracting the BAI value in the centre location of the channel defect from the BAI value of the undisturbed region adjacent to channel defect. A direct correlation was observed between the contrast descriptor ΔBAI and the channel diameter. However, the efficiency of response of ΔBAI to a wider variety of seal defects is still in question for packaging materials and defect types beyond those in the study.

In this study, channel defects (air-filled and water-filled) ranging from 6 to 100 μm in diameter, and solid inclusion defects ranging from 20 to 150 μm in lateral size within the seal region of both plastic trilaminate and aluminium foil pouches were created in the laboratory. Strands from mouse tail tendon as a food-simulating biomaterial were used to generate inclusion defects. The purpose of this study is to evaluate the contrast descriptor, ΔBAI, for two packaging materials and three defect types and sizes.

METHODOLOGY

Sample preparation

All-plastic and foil-containing trilaminate films were used for sample production. These materials are utilized for the production of retort pouches in the food packaging industry.[14] Table 1 shows physical properties of layers in these packaging films. All-plastic trilaminate film (Fuji Tokushu Shigyo Co. Ltd., Seto Aichi, Japan) was transparent while the foil-containing plastic composite (American National Can Company, Chicago, IL) was opaque.

Three types of defects (air-filled channels, water-filled channels and solid inclusions) in the seal region of both all-plastic and foil-containing packages were created. Smooth, die-drawn tungsten wires (California Fine Wire Company, Grover City, CA) with 6, 10, 15, 37, 50, 75 and 100 μm diameters were used to prepare channel defects. To prepare solid inclusion defects; strands of mouse tail tendon, biomaterial to simulate meat fibre and other food fibres were used. These strands were longitudinally extracted from the tails of mice (provided by Beckman Institute's Animal Care Facility, Urbana, IL) under the microscope. After the wire or the strand was located between two facing layers of a packaging film, it was sealed into place by an automatic heat sealer (Doboy, HS-C42051, Doboy, Co., New Richmond, WI). The inner layer of these films, which is the heat sealant layer, was in direct contact with wires and tendon strands, whose longitudinal axes were perpendicular to the sealing direction (termed the seal's major axis in Figure 1(b)). The sealing jaw temperatures for all-plastic and foil-containing films were 132 and 152°C, respectively. Samples were left to cool for at least 5 minutes following the sealing. Air-filled channel defects were prepared by axially removing the wire after cooling. To prepare the water-

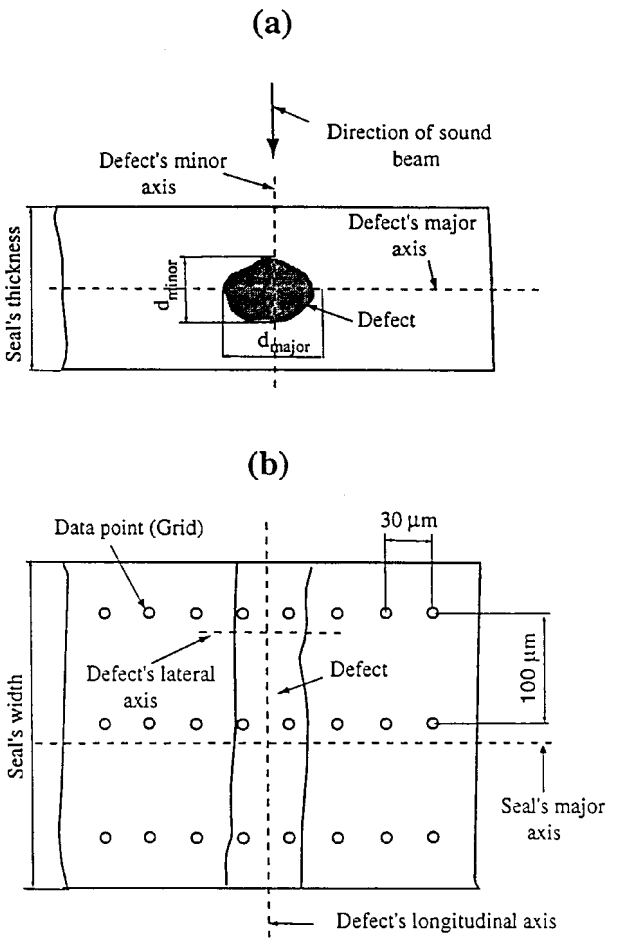

Figure 1. Diagram of a defect sample within the seal region of the package; (a) cross-sectional view; (b) top view.

filled channel defects, samples were immersed into a water bath, and the wire was axially removed. Inclusion defect tendons were left in place. Next, both ends of the channel opening and strand were fused to assure the integrity of the defect's content.

Sample validation

The image of defects was captured using a Nikon Optiphot-2® light transmission microscope, Sony® CCD colour video camera, RasterOps® frame-grabber board, Macintosh IIci® computer and Adobe Photoshop® software. The size of each defect on these images was measured by a calibration grid (Reichert Jung: 2 mm divisions of 10 μm).

The lateral size of the defects was measured by using the top view image. Before measuring the size from the cross-sectional view, samples were cut in the direction parallel to the seal's major axis and transverse to the defect's longitudinal axis. Since the cut surface of samples should be very smooth to identify the defect from its cross-sectional view, it was frozen to −70°C using a deep-freezer (Forma Scientific, Model no. 80478-006, OH) for approximately 30 minutes, and then cut from their midpoint using a cyrostat (Lipshaw Manufacturing Company, Model no. 1500, Detroit, MI), immediately.

System description and data acquisition

Figure 2 shows the major components of the data acquisition system. The defect sample was taped to a plastic holder and placed in a water tank (∼20°C) so that the defect orientation was approximately normal to the sound beam direction (Figure 1(a) and Figure 2). In this system, GPIB (General Purpose Interface Bus) controlled by a C-program communicates with a host PC (ZEOS 66 MHz 486), motor controllers and a pulser–receiver. The mechanical movement of the transducer for scan-

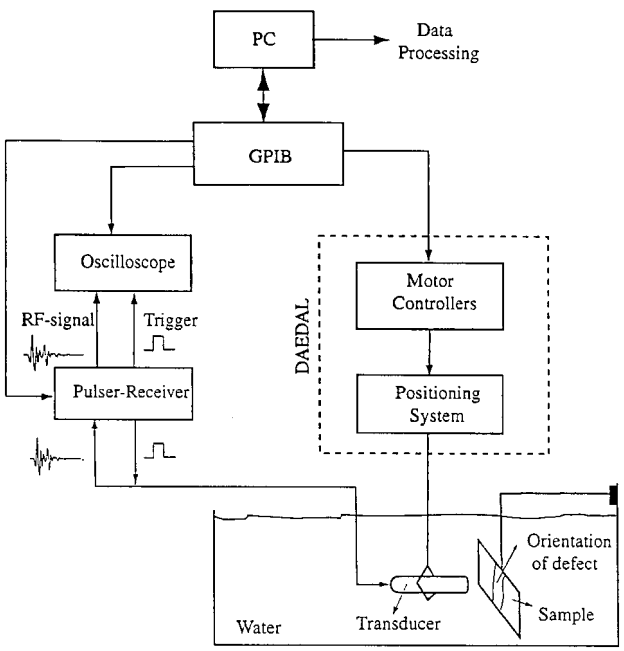

Figure 2. Block diagram of data acquisition system.

ning is achieved by a five-axis (three linear and two rotational) positioning system (Daedal, Inc., Harrison City, PA) that is connected to motor controllers. The linear and rotational position accuracy of the system are 2 μm and 0·01°, respectively. A pulser–receiver (Model 5800, Panametrics, Waltham, MA) was used to generate the 300 V monocycle pulse which excites a spherically focused, 6·35 mm diameter ultrasonic transducer (Panametrics V317, Waltham, MA) with the manufacturer specified centre frequency of 20·0 MHz. The measured centre frequency of the transducer was 17·3 MHz, the focal length was 12·7 mm, the −6 dB depth of focus was 2·42 mm, the −6 dB transmit–receive beam width of focus was 176 um, and the −3 dB fractional bandwidth was 27·4%.[17] The pulser–receiver amplified the received echo signal with 20dB gain, and then it was band-pass filtered (1–35 MHz). Next, this processed radio frequency (RF) echo signal from the pulser–receiver was displayed (500Ms/s) on a digitizing oscilloscope (LeCroy 9354TM, Chestnut, NY) with an eight-bit resolution.

The time-of-transition (*TOT*) of the sound beam at the focal distance in the water was calculated to be 17·16 μs by

$$TOT = \frac{2 \times F}{c_w} \quad (1)$$

where c_w is the speed of the sound in water (1483 m/s)[18] and F is the focal length of the transducer (12·7 mm). The RF waveforms were displayed between TOT = 16·8 and 17·8 μs on the oscilloscope to include the sample thickness (Figure 3). Each RF waveform obtained in this *TOT* range contained 512 data points. In order to establish the orientation of the sample, in which its top surface had to be approximately normal to the transducer, four edges of rectangular sample surface were scanned. As long as all RF waveforms on these edges were within the specified *TOT* range, this meant that the sample was properly positioned. Otherwise, the sample was manually corrected until the signals on edges were within this TOT range.

The sample was scanned in a rectangular grid pattern by moving the transducer with an automatic micro-positioning system (Figure 2). The distances between grids were 30 μm in the direction parallel to the seal's major axis (also transverse to the defect's longitudinal axis) and 100 μm in the direction perpendicular to the seal's major axis (30 μm × 100 μm step sizes) (Figure 1). Field-of-view varied from the smallest 1·5 mm (parallel to seal's major axis) × 1·0 mm (transverse to seal's major axis) to the largest 4·0 mm × 2·0 mm area. If, for example, the size of field-of-view was 1·5 mm × 1·0 mm, then the number of grids in the direction parallel to the seal's major axis would be 50 (1·5 mm/30 μm) and those in the direction transverse to the seal's major axis would be 10 (1·0 mm/100 μm). In the ultrasonic beam direction, each grid contained one RF waveform, and therefore, the total number of waveforms was 500 (10 by 50). As a result, the data set was three-dimensional, and comprised 500 512-point RF data acquisitions for this specific example. After this three-dimensional data set was stored on the PC's hard disk, it was transferred to a SUN Sparc 20 workstation for off-line image processing.

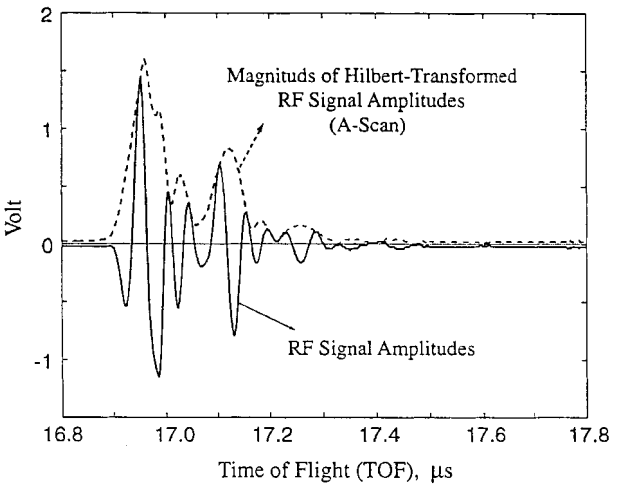

Figure 3. RF waveform and its corresponding Hilbert-transformed magnitudes (A-scan) from the all-plastic film.

BAI-mode imaging

The Backscattered Amplitude Integral (BAI) mode image[10] of each sample was generated by processing the three-dimensional data set. According to this processing technique, each RF waveform is Hilbert-transformed. This step rectifies the RF waveform, and the magnitude of resulting amplitudes yields an envelope[19,20] that represents an A-scan of the corresponding RF waveform (Figure 3).

The BAI value was calculated by integrating the envelope signal (A-scan) between TOT = 16·8 and

17·8 μs. The area under the envelope signal in Figure 3 shows the BAI value for the comparable RF waveform. After the BAI value of each RF waveform was calculated, the three-dimensional data set reduced to a BAI-value matrix. Matrix values were then linearly interpolated by a factor or two in the direction parallel to the seal's major axis (30 μm/2) and by a factor or seven in the direction transverse to the seal's major axis (100 μm/7). After the interpolation, the image pixel size became 14·3 μm × 15·0 μm with the number of rows and columns in the BAI-value matrix being 70 (10 by 7) and 100 (50 by 2), respectively. Next, the interpolated BAI-value matrix was normalized by dividing each BAI value to the maximum BAI-value in the same matrix to generate the grey-scale image. All calculations were performed by MATLAB® (The Math Work, Inc., Natick, Mass).

ΔBAI contrast descriptor

The ΔBAI contrast descriptor has been defined as a measure of contrast in the BAI-mode image of the channel defect[10] and can be described as

$$\Delta\mathrm{BAI} = \mathrm{BAI}_{\mathrm{undisturbed}} - \mathrm{BAI}_{\mathrm{mid\text{-}channel}} \qquad (2)$$

where the $\mathrm{BAI}_{\mathrm{undisturbed}}$ is the unnormalized BAI value from the undisturbed region adjacent to the channel defect, and the $\mathrm{BAI}_{\mathrm{mid\text{-}channel}}$ is the unnormalized BAI value from the centre location of the channel defect. However, this calculation procedure did not produce a stable result for samples produced for this study, i.e., the ΔBAI calculated by equation (2) produced different values at different undisturbed regions. In some instances, the ΔBAI varied by region as much as 200%. The reason for this is that the distance between the undisturbed and the defect region has not been stated clearly in Reference 10. In this study, the ΔBAI contrast value for the defect on the image was calculated by

$$\Delta\mathrm{BAI} = \mathrm{BAI}_{\mathrm{background}} - \mathrm{BAI}_{\mathrm{defect}} \qquad (3)$$

where the $\mathrm{BAI}_{\mathrm{background}}$ is the average unnormalized BAI value of 10 spatially separated random locations from regions, which do not include the defect. The $\mathrm{BAI}_{\mathrm{defect}}$ is the average unnormalized BAI value in the defect location. Figure 4 indicates the background and defect locations on the BAI-mode image. For calculation purposes, 'Imcrop', built-in image processing function in MATLAB®, was used to select the sub-images from the background and defect locations. Individual sub-image areas were 0·3 mm × 0·3 mm, and 10 different sub-images were used to estimate the $\mathrm{BAI}_{\mathrm{background}}$ value. The same procedure was followed for the calculation of the $\mathrm{BAI}_{\mathrm{defect}}$; however, only one sub-image was selected which longitudinally covered the defect region.

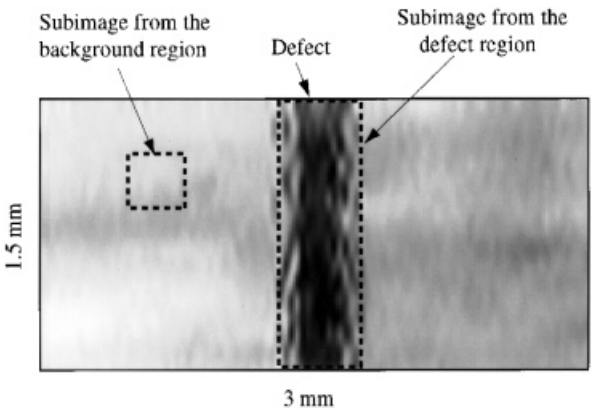

Figure 4. A 17·3 MHz BAI-mode image of water-filled channel defect (38 μm) in the seal region of all-plastic film. Dashed rectangles are used to calculate the contrast descriptor, ΔBAI, of the defect.

Statistical analysis

Regression analysis between the size of defects and ΔBAI contrast values for each defect type was executed. Statistical calculations were performed by the built-in functions in Microsoft Excel® 97.

RESULTS AND DISCUSSION

Channel defects were classified as: air-filled channel defect within all-plastic film (ACP), water-filled channel defect within all-plastic film (WCP), air-filled channel defect within foil-containing film (ACF) and water-filled channel defect within foil-containing film (WCF). Since seven different tungsten wires (6, 10, 15, 38, 50, 75 and 100 μm) were used to create these defects, and since five replications for each wire size were produced, 35 channel defects were fabricated for each group. Thus, a total of 140 channel defect samples were evaluated. Also, 18 inclusion defects

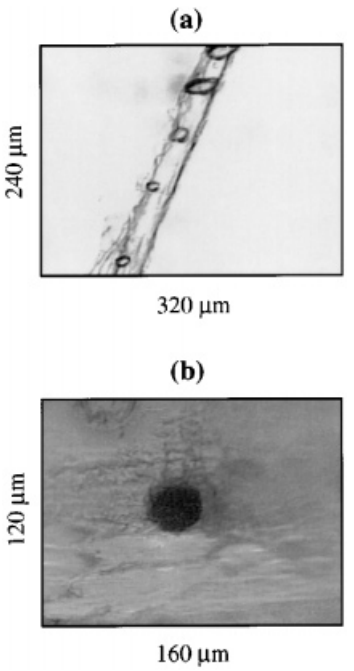

Figure 5. Light microscope images; (a) top view of inclusion defect (minimum lateral size = 29·8 μm); (b) cross-sectional view of air-filled channel defect (36·8 μm) in the seal region of all-plastic films.

within all-plastic (IDP) and 15 inclusion defects within foil-containing film (IDF) were evaluated.

Lateral size measurement

Owing to the opaque nature of foil-containing films (ACF, WCF and IDF), the lateral size of the defect in these samples could not be optically measured. Only the lateral size of ACP, WCP and IDP samples was measured (Figure 5(a)). The lateral size fraction (f_{lateral}) was calculated for ACP and WCP samples by

$$f_{\text{lateral}} = \frac{d_{\text{lateral}}}{d_{\text{wire}}} \tag{4}$$

where the d_{lateral} is the lateral size of the defect (μm) measured using the light microscope image, and the d_{wire} is the diameter of the tungsten wire used to create the defect. The f_{lateral} was $0{\cdot}91 \pm 0{\cdot}06$ for the 70 samples tested. Consequently, these channels' lateral size was apparently smaller than the size of the tungsten wires used to create the respective defects.

The lateral size of 18 inclusion-defect samples (IDP) was also measured. Since the tendon strands' shape changed throughout their longitudinal axis, the size measured on their lateral axis also varied (Figure 1(b)). Therefore, the smallest lateral size of IDP samples was measured, and it varied between 15 and 130 μm.

Optical size measurements from the cross-section

Although foil-containing films were opaque from the top view for lateral size measurements, defects in this material and all-plastic films could be measured from the cross-section under the light transmission microscope (Figure 5(b)). 140 channel defect samples (ACP, WCP, ACF and WCF) were tested; however, 33 of them could not be measured under the microscope. Of these unidentified samples, 24 of them were the channel defects created by 6 and 10 μm diameter tungsten wires. The smearing of the packaging material on the cut surface did not allow the detection of particularly small defects ($\leqslant$10 μm). The cross-sectional channel shape of the defect was elliptical for all other 107 identified samples. To measure the eccentricity of the elliptic geometry of the defect, the fraction f_{defect} was defined by

$$f_{\text{defect}} = \frac{d_{\text{major}}}{d_{\text{minor}}} \tag{5}$$

where the d_{major} is the size on the major defect axis, and the d_{minor} is the size on the minor defect axis (Figure 1(a)). The f_{defect} was $1{\cdot}16 \pm 0{\cdot}14$ for the 107 identified samples, and it ranged from 0·88 to 1·76.

All inclusion defects—18 IDP and 15 IDF—were measured from their cross-sections, and the shape of these defects was also elliptical. The f_{defect} of these samples was $2{\cdot}14 \pm 0{\cdot}81$, and it ranged from 1·02 to 3·72, which clearly indicated that the d_{major} of tendon strands was much larger than their d_{minor} compared with channel defect samples. Furthermore, the d_{major} of these defects ranged from 20 to 150 μm, and the minimum detected d_{major} for IDP and IDF samples was 20 and 26·4 μm, respectively. The reason for the expansion of these defects through the major axis might be the blade of cyrostat (used to cut samples for size measurements) that squeezed the sample from the top.

For definition purposes, the d_{major} is the value quoted hereafter for the size of both channel

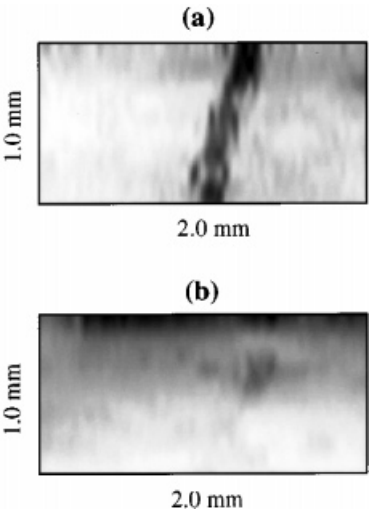

Figure 6. (a) 17·3 MHz BAI-mode image of detected air-filled channel defect (d_{major} = 6 μm) in the seal region of foil-containing film; (b) 17·3 MHz BAI-mode of undetected water-filled channel defect (d_{major} = 6 μm) in the seal region of all-plastic film.

defects and inclusion defects. As explained in earlier discussion, some of the channel defects (33 of them) could not be identified from their cross-sectional view. For these samples, the defect diameter will be referred to by the forming-wire size.

The BAI-mode imaging technique has the capability of subwavelength detection of channel and inclusion defects, e.g., detection of defects in sizes below 100 μm whereas λ ($= c/f$) is 138 μm for all-plastic films and 142 μm for foil-containing films at the centre frequency of 17·3 MHz. All tendon strands and channels ($d_{major} > 15$ μm) were easily detected on the BAI-mode image. However, some small channel defects ($d_{major} \leqslant 15$ μm) did not produce the same efficient results. Figure 6 shows two example BAI-mode images to indicate the difference between the detected and undetected defects. Table 2 shows the number of defect samples that were not detected on the BAI-mode images. For easy illustration purposes, the diameter of the wire was grouped instead of the real defect size (d_{major}). The detection failure of defects (as percentage) was calculated for the corresponding wire group, which generated a total of 20 samples. This failure increased from 20% for defects produced by 15 μm diameter wires to 70% for those produced by 6 μm diameter wires. These results indicate that the BAI-mode resolution decreased dramatically as the size of these defects decreased.

Figures 4 and 6(a) demonstrate that the contrast of the defect region on the image is different from that of the undisturbed region, and this result was consistent for all BAI-mode images that apparently demonstrated the defect. The BAI values in the defect region were smaller than those in the undisturbed region, i.e., the total reflected echo energy from the defect region was lower than that of the undisturbed region. In addition, the size of defects on the BAI-mode image was much larger than its actual size (d_{major}) and varied approximately between 150 and 200 μm. The magnifica-

Table 2. Unidentified channel defects ($\leqslant$15 μm) on BAI-mode images

Wire used to create the channel defect (μm)	Types of packaging material: All-plastic trilaminate, Channel type: Air*	All-plastic trilaminate, Channel type: Water*	Foil-containing trilaminate, Channel type: Air*	Foil-containing trilaminate, Channel type: Water*	Percentage of unidentified† channel defects on the BAI-mode image (%)†
15	0	0	2	2	20
10	3	2	2	3	50
6	5	4	2	3	70

*Column represents a total number of unidentified channel defects out of five replications.
† The percentage was calculated by 100 × total number of unidentified images for the given wire type/20.

Packaging Technology and Science

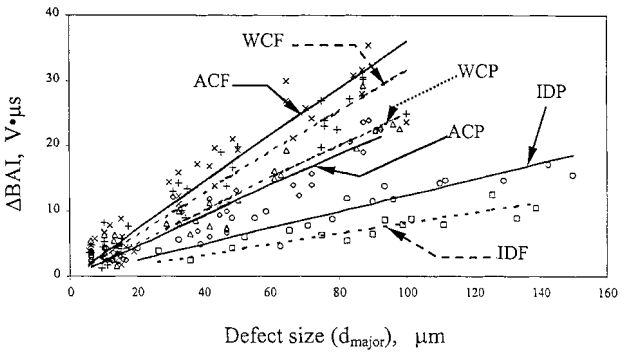

Figure 7. The size of defects versus ΔBAI (×: ACF, +: WCF, △: WCP, ◇: ACP, ○: IDP, □: IDA). The line-fit of each group was drawn according to its regression constants in Table 3.

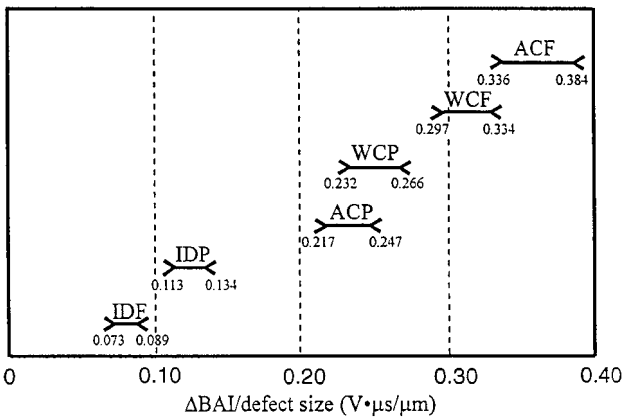

Figure 8. 95% confidence intervals of the slope of fitted lines in Figure 7.

tion of defects in the image was consistent with the −6 dB transmit–receive beam width (176 μm) of the 17·3 MHz centre frequency transducer used in this study. Similar results have also been obtained by recent studies.[10,11]

Figure 7 shows the relationship between the ΔBAI value and the defect size. The relationship of ΔBAI values with their respective defect sizes showed a linear correlation for each sample group (ACP, WCP, ACF, WCF, IDP and IDF). Table 3 indicates the slope of fitted lines (defect size versus ΔBAI) and the corresponding correlation coefficient (R^2) obtained by the linear regression. The fitted lines in Figure 7 were drawn according to results obtained by the regression analysis. High correlation coefficients clearly indicate that the ΔBAI contrast value decreased as the defect size decreased, i.e., BAI values in the defect region (BAI_{defect}) became close to those in the background region ($BAI_{background}$) as the defect size declined.

Table 3. Slope of fitted lines (d_{major} versus ΔBAI) in Figure 8 and correlation coefficients obtained by linear regression analysis

Sample group	Slope (V·s/m)	Correlation coefficient (R^2)
ACP	0·233	0·91
WCP	0·250	0·89
ACA	0·359	0·88
WCA	0·317	0·91
IDP	0·124	0·79

Figure 8 demonstrates the 95% confidence interval of the slope ($\Delta BAI/d_{major}$) of the fitted lines in Figure 7. The right arrow (>) and the left arrow (<) in Figure 8 indicate the lower and upper limit of confidence intervals, respectively. According to this figure, only the confidence intervals of WCP and ACP samples, i.e., channel defects in the seal region of all-plastic films, overlap each other. Consequently, at a 95% confidence level the ΔBAI values of WCP samples were not significantly different from those of ACP samples for the same d_{major}. On the other hand, ΔBAI values of other samples were significantly different from each other for the same d_{major}. As a result, the contrast descriptor, ΔBAI, varied with defect types (air-filled channels, water-filled channels and inclusion defects), defect sizes (d_{major}) and types of packaging materials (all-plastic and foil-containing films).

Since some of channel defect samples ($d_{major} \leqslant 15$ μm), as discussed earlier, were not identifiable, the calculation of the ΔBAI without knowing the exact location of the defect was impossible for these samples. A new technique in a recent study,[21] which uses the same three-dimensional data set used in the BAI-mode imaging, has the ability of detecting the small defects that the BAI-mode imaging could not identify. This new high-contrast image technique looks like C-mode imaging. However, unlike the conventional C-scan processing which includes

only a portion of the sample, the signal has been processed differently before constructing the image (refer to Reference 21). After placing the image obtained by this technique and the BAI-mode image side by side, the location of the defect on the BAI-mode image was determined, and consequently, the ΔBAI contrast values of these unidentified samples were calculated.

CONCLUSION

The ΔBAI technique can be used in two ways. First, the BAI-mode image is limited for characterizing the defect in terms of its size. However, by knowing the packaging material's characteristics and by estimating what kind of defect might be involved to contaminate the seal region of the package, the size of the defect can be approximated using the calibration curve (Figure 8—ΔBAI versus defect size). Different defects have different impacts on the ΔBAI value for the same packaging material. After recognizing all significant defect types within the seal region of a packaging material, the calibration curves can be prepared in the laboratory for use by on-line equipment.

Second, the ΔBAI contrast descriptor on the BAI-mode image can provide a quite effective sensing method for package inspection, and may do so with less equipment and complexity than the laboratory studies have required. After the minimum defect size is safely identified by the BAI-mode image (15 μm in this study), the corresponding minimum ΔBAI contrast value can be set. This minimum value would provide stable and robust criteria (relative to human visual judgement of the package exterior) for deciding whether the package is rejected from the inspection line or not. Application of results in this study to on-line inspection will require further research. The calculation of a ΔBAI contrast descriptor is currently limited by manual data collection algorithms. A technique which automatically recognizes the defect on the BAI-mode image, and automatically calculates the ΔBAI contrast descriptor is necessary for practical automatic data collection and calibration curve construction purposes.

ACKNOWLEDGEMENTS

The authors gratefully acknowledge the professional assistance with the sample validations by James F. Zachary, Department of Veterinary Pathobiology, University of Illinois.

This work was supported in part by the Value-Added Research Opportunities Program, Agricultural Experiment Station, University of Illinois.

REFERENCES

1. R.A. Lampi, G.L. Schulz, T. Ciavarani and P.T. Burke, *Food Technology*, **30**, 38–48 (1976).
2. V. Gnanasekharan and J.D. Floros, *Packaging Technology & Engineering*, **3**, 44–48 (1994).
3. R.K. Singh and P.E. Nelson, *Advances in Aseptic Processing Technologies*, Elsevier Applied Science, New York, 1992.
4. B.A. Blakistone and C.L. Harper (Ed.), 'Plastic Package Integrity Testing Assuring Seal Quality'. *Institute of Packaging Professionals*, Herndon, VA, USA, 1995.
5. C.L. Harper, B.S. Blakistone, J.B. Litchfield and S.A. Morris, *Food Technology*, **6**, 336–340 (1995).
6. D. Jarman, B. Farahbakhsh and R. Herzig, US Patent no. 5,372,042. 'Ultrasonic inspection of seal integrity of bond lines in sealed containers.' (1994).
7. C.L Harper, 'A microbial challenge procedure for identification of defective flexible plastic pouch seals.' Ch. 10 in *Plastic Package Integrity Testing Assuring Seal Quality*, B.A. Blakistone and C.L. Harper (Ed.), p. 79–82. *Institute of Packaging Professionals*, Herndon, VA, USA, 1995 op. cit.
8. B.A. Blakistone, S.W. Keller, J.E. Marcy, G.H. Lacy, C.R. Hackney and W.H. Carter, Jr., *Journal of Food Protection*, **59**, 764–767 (1996).
9. A.A. Safvi, H.J. Meerbaum, S.A. Morris, C.L. Harper and W.D. O'Brien, Jr., *Journal of Food Protection*, **60**, 309–314 (1997).
10. K. Raum, A. Ozguler, S.A. Morris and W.D. O'Brien, Jr., *IEEE Transactions on Ultrasonics, Ferroelectrics, and Frequency Control*, **45**, 30–40 (1998).
11. A. Ozguler, S.A. Morris and W.D. O'Brien, Jr., 'Ultrasonic Imaging of Micro-Leaks and Seal Contamination in Flexible Food Packages by the Pulse Echo Technique.' *Journal of Food Science*, **63**, 673–678 (1998).
12. United States Code of Federal Regulations. Published by the Office of the Federal Register. Available from the superintendent of Documents, U.S. Government Print Office, Washington, DC 20402.
13. W.E. Woodson and D.W. Conover, *Human Engineering Guide For Equipment Designers*, University of California Press, Berkely, CA, 1964.
14. T. Kadoya, *Food Packaging*, Academic Press, Inc., San Diego, CA, 1990.

15. W.A. Jenkins and J.P. Harrington, *Packaging Foods with Plastics*, Technomic Publishing Company, Inc., Lancaster, PA, 1991.
16. A.R. Selfridge, *IEEE Transactions on Sonics and Ultrasonics*, **SU-32**, 381–395 (1985).
17. K. Raum and W.D. O'Brien, Jr., *IEEE Transactions on Ultrasonics, Ferroelectrics and Frequency Control*, **44**, 810–815 (1997).
18. W.D. Wilson, *J. Acoust. Soc. Amer.*, **31**, 1067–1072 (1959).
19. G.G. Leisk and A. Saigal, *Material Evaluation*, **54**, 840–843 (1996).
20. A.V. Oppenheim and R.W. Schafer, *Digital Signal Processing*, Prentice Hall, Englewood Cliffs, NJ, 1975.
21. C.H. Frazier, A. Ozguler, S.A. Morris and W.D. O'Brien, Jr., 'High-Contrast Imaging of Defects in Food Package Seals'. *IEEE 1997 Ultrasonics Symposium*, Toronto, Ontario, (10/7/97).